Isosbestic Points in the Spectral Function of Correlated Electrons*

Martin Eckstein, Marcus Kollar, and Dieter Vollhardt

Theoretical Physics III, Center for Electronic Correlations and Magnetism, Institute for Physics, University of Augsburg, 86135 Augsburg, Germany
E-mail: Dieter.volhardt@physik.uni-augsburg.de

We investigate the properties of the spectral function $A(\omega, U)$ of correlated electrons within the Hubbard model and dynamical mean-field theory. Curves of $A(\omega, U)$ versus ω for different values of the interaction U are found to intersect near the band-edges of the non-interacting system. For a wide range of U the crossing points are located within a sharply confined region. The precise location of these "isosbestic points" depends on details of the non-interacting band structure. Isosbestic points of dynamic quantities therefore provide valuable insights into microscopic energy scales of correlated systems.

PACS Numbers: *71.27.+a.*

1. INTRODUCTION

A family of non-monotonic curves, obtained by plotting a quantity $f(x, y)$ as a function of one of its variables (say, x) for different values of y, will in general intersect. The crossing points are located along a curve $x^*(y)$ defined by

$$\left.\frac{\partial f(x, y)}{\partial y}\right|_{x^*(y)} = 0. \tag{1}$$

In physics, chemistry and biology these crossing points are sometimes found to be confined to a remarkably narrow region, or even located at a single point,[1] thus leading to a conspicuous feature termed *isosbestic point*.[2,3] In the former case x^* depends only weakly on y, while in the latter case x^* does not depend on y at all.

*This paper is dedicated to Hilbert von Löhneysen on the occasion of his 60th birthday.

For example, the curves of the specific heat $C(T, X)$ versus temperature T of numerous strongly correlated fermionic systems are known to cross once or twice when plotted for different values of a second thermodynamic variable X.[4] In particular, crossing points are observed for different pressures ($X = P$) in normalfluid ^{3}He (Fig. 1(a))[5] and heavy-fermion systems such as $CeAl_3$ (Fig. 1(b)).[6] By changing the magnetic field ($X = B$) the same feature is seen in heavy-fermion compounds such as $CeCu_{6-x}Al_x$ (Fig. 1(c)).[7]

Crossing points of specific heat curves are also observed in lattice models for correlated electrons such as the one-band Hubbard model

$$H = \sum_{ij\sigma} t_{ij}\, c^{\dagger}_{i\sigma} c_{j\sigma} + U \sum_{i} n_{i\uparrow} n_{i\downarrow} - \mu \sum_{i\sigma} n_{i\sigma}, \tag{2}$$

where $c^{\dagger}_{i\sigma}$ are creation operators for an electron at site i with spin σ and $n_{i\sigma} = c^{\dagger}_{i\sigma} c_{i\sigma}$ are density operators. The model contains the hopping amplitude t_{ij}, the local Coulomb interaction U, and the chemical potential μ as parameters. At half-filling the curves $C(T, U)$ versus T always cross at two temperatures. This is observed, for example, in the case of nearest–neighbor hopping in $d = 1$,[8,9] $d = 2$,[10] and $d = \infty$ (Fig. 1(d)),[11] as well as for long-range hopping in $d = 1$.[12]

As shown in Ref. 4 the existence of crossing points in the specific heat curves, and the fact that they may be quite sharp, can be linked (i) to a sum rule for the change of the entropy $S(T, X)$ with respect to X in the limit of $T \to \infty$, and (ii) the properties of the susceptibilities $\chi^{(n)}(T, X) = \partial^n \xi / \partial X^n$, where $\xi(T, X)$ is the conjugate variable to X. Furthermore, the fact that the high-temperature crossing point in $C(T, U)$ for the one-band Hubbard model occurs at a nearly universal value $C^*/k_B \simeq 0.34$ was shown to be a consequence of the existence of two small parameters: the integral over the deviation of the density of states from a constant value, and the inverse dimension, $1/d$.[13]

The isosbestic points discussed above all appear in curves of the specific heat $C(T, X)$ versus temperature T when plotted for different values of another thermodynamic variable X. On the other hand, such points are known to occur also in dynamic quantities, e.g., in the optical conductivity $\sigma(\omega, n)$ of the high-T_c material $Nd_{2-x}Ce_xCuO_{4-y}$ where n is the density or doping (Fig. 1(e)),[14] and in the Raman response $\chi(\omega, T)$ calculated by means of the Hubbard model[15] and the Falicov–Kimball model.[16] In general, there is no reason for the intersection of these curves to occur at one sharp frequency ω^*, i.e., to be completely independent of any other parameter defining the family of curves. There are, however, at least two classes of isosbestic points which are genuinely point-like. One is the exact

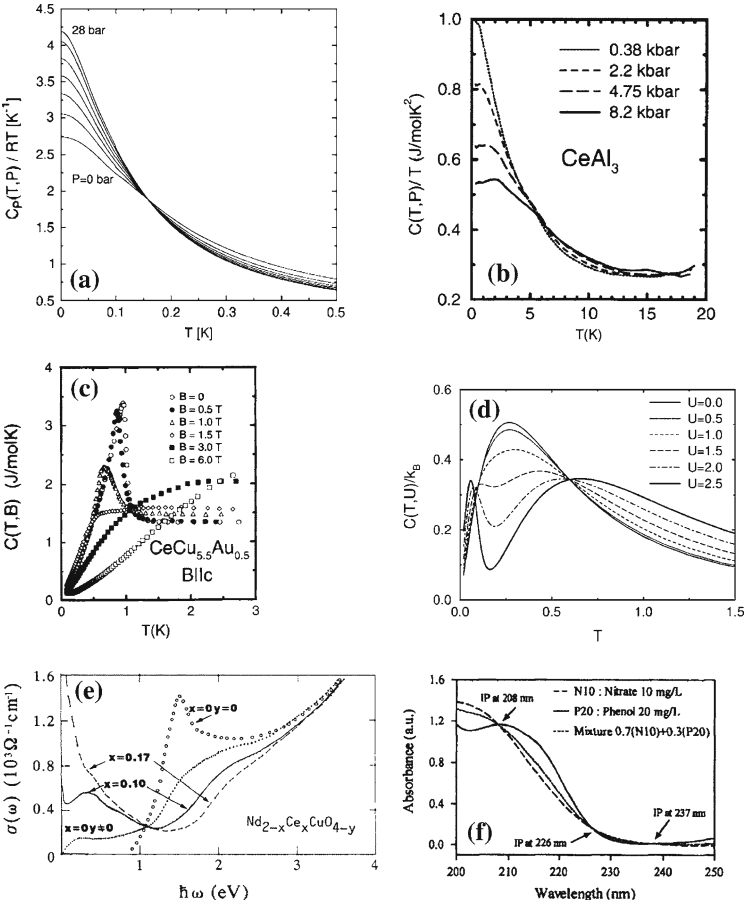

Fig. 1. Examples of crossing points in various correlated systems: (a) Specific heat of normal liquid ^{3}He measured at different pressures[5] (after Ref. 4). (b) Specific heat of $CeAl_3$ measured at different pressures[6](after Ref. 4). (c) Specific heat of $CeCu_{5.5}Au_{0.5}$ measured at different magnetic fields[7] (after Ref. 4). (d) Specific heat of the Hubbard model calculated for different interactions[11] (after Ref. 4). (e) Optical conductivity of $Nd_{2-x}Ce_xCuO_{4-y}$ measured at different doping (after Ref. 14). (f) Isosbestic point in ultraviolet spectra of three solutions of phenol and nitrate (after Ref. 18).

crossing of curves described by a scaling function in critical phenomena; see, for example, the crossing of conductance curves near the Anderson transition.[17] Another one is found in optical spectroscopic studies[1,2,18] of systems consisting of two components with densities n_a, n_b and $n = n_a + n_b = \text{const}$. In this case, the absorbance as a function of frequency $\alpha(\omega, n_a)$

depends only linearly on the density, i.e., has the special form

$$\alpha(\omega, n_a) = n_a f_a(\omega) + (n - n_a) f_b(\omega). \tag{3}$$

If f_a and f_b coincide at a frequency ω^*, i.e., $f_a(\omega^*) = f_b(\omega^*)$, then

$$\left.\frac{\partial \alpha(\omega, n_a)}{\partial n_a}\right|_{\omega^*} = 0. \tag{4}$$

This implies that for all densities n_a the absorbance curves intersect at one frequency ω^* (or the equivalent wave length, Fig. 1(f)). Similar isosbestic points are found in diffraction experiments on glasses.[19] Quite generally, whenever a system is a superposition of two (or more) components such that its dynamic quantities, e.g., the dynamic conductivity or a response function, have the form described by Eq. (3), isosbestic points are bound to occur. This applies in particular to any kind of two-fluid model employed, for example, in phenomenological theories of superconductivity and superfluidity. There the density of the two components (e.g., the normal and superfluid component) depend on temperature while the total density is constant: $n = n_a(T) + n_b(T) = \text{const}$. Properties of the system are then described by the superposition of the two components, leading to a special dependence of quantities $f(T, X)$ on T and X of the form

$$f(T, X) = n_a(T) f_a(X) + [n - n_a(T)] f_b(X). \tag{5}$$

This implies the crossing of curves for different temperatures T at a single point X^* determined by $f_a(X^*) = f_b(X^*)$. Whether the surprisingly sharp isosbestic points found, for example, in the optical conductivity of $Nd_{2-x}Ce_xCuO_{4-y}$ (Fig. 1(e))[14] can be explained in this way still has to be investigated.

Disregarding critical phenomena with scaling behavior and the special linear dependence given by Eq. (3), isosbestic points in *dynamical* quantities of correlated electron systems have so far only been noticed but never explained. As in the case of the crossing of specific heat curves there are two separate questions to be answered: (i) Why do curves of frequency-dependent quantities cross at all, and (ii) under what circumstances is the crossing region confined to a narrow region, or is even point-like? In analogy to the entropy sum rule in the case of specific heat curves, a good starting point for such an investigation is the study of *frequency sum rules*. Examples are the f-sum rule for the dynamical conductivity and sum rules involving the spectral function.

In this paper, we investigate crossing points in frequency by studying a particularly basic quantity—the local (momentum-integrated) spectral

function $A(\omega, U)$ of the Hubbard model, a quantity which obeys fundamental frequency sum rules. In the following we will write $A(\omega, U) \equiv A(\omega)$; the parameter U will only be written when explicitly needed. For simplicity we will employ the Bethe lattice in the limit of infinite coordination number. In this case the self-energy Σ becomes local and can be calculated using dynamical mean-field theory (DMFT).[20–25] In Sec. 2.1., we discuss the behavior of $A(\omega)$ and in Sec. 2.2. the location of crossing points. Their behavior at small interaction is studied in Sec. 3. We use weak-coupling perturbation theory (Sec. 3.1.) to investigate how the crossing points of $A(\omega)$ depend on the non-interacting bandstructure and the interaction strength U. This is performed for both the Bethe lattice (Sec. 3.2.) and a model density of states (Sec. 3.3.), which differ in their van-Hove singularities. A conclusion in Sec. 4. closes the paper.

2. CROSSING POINTS OF THE SPECTRAL FUNCTION

2.1. Spectral Function in DMFT

We consider the paramagnetic phase of the Hubbard model (2) in DMFT.[20–25] In this case Σ does not have any site- or spin-dependence, and the local Green function $G(\omega)$ becomes

$$G(\omega) = G_0(\omega + \mu - \Sigma(\omega)). \tag{6}$$

The non-interacting Green function $G_0(z)$, written as a function of the complex variable z, is given by the Hilbert transform of the non-interacting density of states (DOS) $\rho(\epsilon)$,

$$G_0(z) = \int d\epsilon \frac{\rho(\epsilon)}{z - \epsilon}. \tag{7}$$

The local spectral function $A(\omega)$ is then given by

$$A(\omega) = -\frac{1}{\pi} G''(\omega + i0). \tag{8}$$

(We use single and double primes to indicate real and imaginary part of a complex quantity.) In Fig. 2, the spectral function is plotted for various U in the case of half-filling. The numerical data are taken from Ref. 26, where the effective impurity problem was solved with numerical renormalization group (NRG). As usual for model calculations within DMFT the semi-elliptic Bethe DOS

$$\rho(\epsilon) = \frac{2}{\pi W} \sqrt{1 - \frac{\epsilon^2}{W^2}}, \quad W = 1 \tag{9}$$

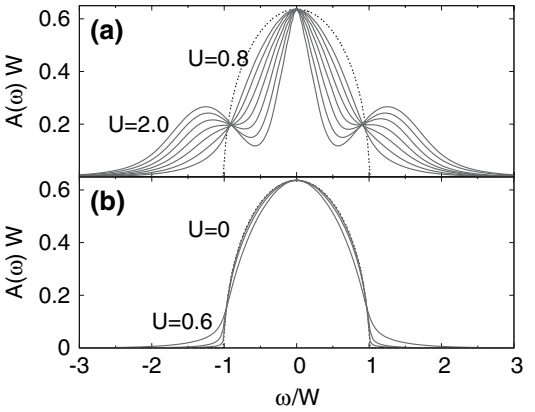

Fig. 2. (Color online) Spectral function of the Hubbard model, calculated with DMFT for the Bethe DOS [Eq. (9)]; the data are from Ref. 26, (a) Sharp crossing points (isosbestic points) occur for intermediate U ($U/W = 0.8, 1.0, \ldots, 2.0$). (b) For small U the crossing points move up and inward as U is increased ($U/W = 0.2, 0.4, 0.6$).

with half-bandwith W was used as non-interacting DOS; we set $W = 1$ as energy scale.

For the values of U in Fig. 2 the system is assumed to be in the Fermi-liquid phase. As the interaction increases, spectral weight is redistributed from the vicinity of the Fermi level to the Hubbard subbands which are peaked at frequency $\omega \approx \pm U/2$, and the well-known three-peak structure of the spectral density emerges. The central spectral peak vanishes at the metal–insulator transition, which occurs at $U = 2.92\,W$.[27,28]

2.2. Crossing Points

There are three crossing points visible in Fig. 2. The first one, at $\omega = 0$, has a simple explanation: In infinite dimensions Luttinger's theorem entails that the chemical potential μ in the interacting system must be shifted according to[29]

$$\mu = \mu_0 + \Sigma(0) \tag{10}$$

in order to keep the number of particles fixed, where μ_0 is the Fermi energy for the non-interacting system with the same number of particles. Thus, the value of the Green function $G(\omega) = G_0(\omega + \mu - \Sigma(\omega))$ at the Fermi level is independent of U in the metallic phase, and the crossing point at $\omega = 0$ is exact. That the curves do not really cross but only touch is a consequence of the particle-hole symmetry at half-filling, which

implies $A(\omega) = A(-\omega)$. For any other density or an asymmetric DOS there is a true crossing point at $\omega = 0$.

The other two crossing points of $A(\omega)$ are situated at $\omega \approx \pm 1$. In contrast to the pinning at $\omega = 0$, their explanation is more complicated. The crossing region at $\omega \approx \pm 1$ is very narrow for intermediate values of U ($0.8 \lesssim U/W \lesssim 2.0$, Fig. 2(a)). For smaller values of U (Fig. 2(b)), we observe that the region of crossing points is less confined. The crossing points move up and inward as U is increased. However, as shown below the crossing *frequency* does not depend strongly on U up to $U \approx 2$. Similar crossing points are found in the spectral function of the Falicov–Kimball model.[16]

Let us first establish that curves $A(\omega, U)$ vs. ω for different values of U always cross at some frequency ω^*, defined by

$$\left.\frac{\partial A(\omega, U)}{\partial U}\right|_{\omega^*(U)} = 0. \tag{11}$$

That two such curves *must* cross follows from the sum rules

$$\int_{-\infty}^{0} d\omega A(\omega, U) = \frac{n}{2}, \tag{12}$$

$$\int_{-\infty}^{\infty} d\omega A(\omega, U) = 1, \tag{13}$$

where n is the density. The derivatives of these equations with respect to U yields

$$\int_{-\infty}^{0} d\omega \frac{\partial A(\omega, U)}{\partial U} = \int_{0}^{\infty} d\omega \frac{\partial A(\omega, U)}{\partial U} = 0 \tag{14}$$

and thus $\partial A(\omega, U)/\partial U$ vanishes either identically or changes sign at least at one point in each of the intervals $(-\infty, 0)$ and $(0, \infty)$. This is the location of the crossing point.

However, the existence of a solution to Eq. (11) is not sufficient for the observation of a sharp crossing point as in Fig. 2(a). In general the crossing frequency ω^*, and also the value $A^* \equiv A(\omega^*(U), U))$ of $A(\omega)$ at this point depends on U. This becomes directly evident from Fig. 3, where $\omega^*(U)$ and $A^*(U)$ are plotted as a function of U. Since these data were obtained from the intersections of curves $A(\omega, U)$ differing by $\Delta U = 0.1\,W$, while a solution to Eq. (11) corresponds to taking $\Delta U \to 0$, they have to be understood as rather rough estimates for ω^* and A^*. Furthermore, the resolution of the NRG data at $\omega = \pm W$ is already much lower than in the vicinity of the Fermi level. Nevertheless, Fig. 3 clearly shows that the strong variation of A^* with U (for small U) causes the crossing region

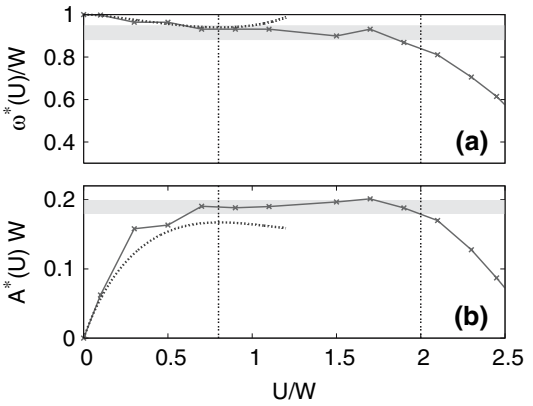

Fig. 3. (Color online) (a) The crossing point $\omega^*(U)$ of the spectral function for the half-filled Hubbard model as a function of U and (b) $A^*(U)$, the value of $A(\omega)$ at this point. Each data point corresponds to the intersection of two neighboring curves shown in Fig. 2. The dotted lines delimit the range of U in Fig. 2(a) and (b), and the shaded bars mark the corresponding width of the crossing region Fig. 2(a). Dotted curves are the result of second-order perturbation theory (Sec. 3.). Due to particle-hole symmetry of the half-filled system it is sufficient to consider only $\omega > 0$.

to become much narrower when only intermediate U are plotted as in Fig. 2(a). By contrast, the value of ω^* remains close to the non-interacting band-edge $\omega = W$ for all U up to $U \approx 2\,W$.

The variation of A^* and ω^* with U, i.e., the derivatives $d\omega^*/dU$ and dA^*/dU are not independent. The latter is given by

$$\frac{dA^*}{dU} = \left.\frac{\partial A(\omega, U)}{\partial U}\right|_{\omega^*} + \left.\frac{\partial A(\omega, U)}{\partial \omega}\right|_{\omega^*} \frac{d\omega^*}{dU} \tag{15}$$

and since the first term vanishes by definition [Eq. (11)] we obtain the basic relation

$$\frac{dA^*}{dU} = \left.\frac{\partial A(\omega, U)}{\partial \omega}\right|_{\omega^*} \frac{d\omega^*}{dU}. \tag{16}$$

In the present case $d\omega^*/dU$ is small for all $U < 2W$, while the derivative $\partial A/\partial\omega|_{\omega^*}$ diverges as U approaches zero. This is because $A(\omega)$ approaches the non-interacting DOS $\rho(\epsilon)$ [Eq. (9)] and ω^* moves to the band-edge where $\rho(\epsilon)$ has a van-Hove singularity. Thus an almost constant crossing frequency ω^* is not in contradiction to a large variation of $A^*(U)$.

3. CROSSING POINTS AT WEAK COUPLING

As discussed above, well-defined crossing points in $A(\omega)$ exist not only at intermediate U (Fig. 2(a)) but also at small U (Fig. 2(b)). We now investigate the behavior of ω^* in the limit of small U by means of many-body weak-coupling perturbation theory (Sec. 3.1.). We first show that ω^* approaches the band-edge as $\omega^* = 1 + \mathcal{O}(U^2)$ if there is a van-Hove singularity at the band-edge (i.e., a divergent slope of $\rho(\epsilon)$, see Sec. 3.2.), and later contrast this by considering a DOS which vanishes linearly at the band-edge (Sec. 3.3.).

3.1. Weak-coupling Perturbation Theory

We start with a short summary of weak-coupling perturbation theory for the local Green function in the paramagnetic phase of the Hubbard model. For $U \ll W$ one can use a perturbative expansion

$$\Sigma(\omega) = \sum_{n \geq 1} U^n \Sigma_n(\omega) \tag{17}$$

for the self-energy Σ, where the functions $\Sigma_n(\omega)$ are given by the sum over all irreducible Feynman diagrams with n vertices. It is convenient to perform this expansion relative to the Hartree approximation.[30] The series (17) is then rearranged such that each line in the Feynman diagrams for Σ_n is replaced by the Hartree expression for the Green function, and in turn all Feynman diagrams which contain first-order self-energy insertions are omitted. Then Σ_1 is just given by the static Hartree self-energy $\Sigma_H = Un/2$, and only a single Feynman diagram contributes to $\Sigma_2(\omega)$.

In the following we discuss only the case $\mu = U/2$, for which the Hubbard model on a bipartite lattice becomes half-filled and particle-hole symmetric. This entails a number of important simplifications:[31] All odd terms in Eq. (17) apart from Σ_H vanish and for the even terms the symmetry relations $\Sigma_n'(\omega) = -\Sigma_n'(-\omega)$ and $\Sigma_n''(\omega) = \Sigma_n''(-\omega)$ hold, so that $\Sigma(0) = \Sigma_H = U/2$. This is of course consistent with Eq. (10).

The calculation of diagrams is considerably simplified in infinite dimensions, where multidimensional momentum integrals can be reduced to one-dimensional integrals over the non-interacting density of states. For further reference we mention a convenient expression for the second-order diagram. In case of particle-hole symmetry $\Sigma_2(\omega)$ can be written as[30]

$$\Sigma_2(\omega) = \text{  } = -i \int_{-\infty}^{\infty} d\lambda\, e^{i\lambda z} [2A'(\lambda)^3 - 6A''(\lambda)^2 A'(\lambda)], \tag{18}$$

where

$$A(\lambda) = \int_{-\infty}^{\infty} d\xi \, e^{-i\lambda\xi} \rho(\xi) f(\xi) \tag{19}$$

and $f(\xi) = 1/(e^{\beta\xi} + 1)$ is the Fermi function.

3.2. Bethe Density of States

As a representative of a DOS with a van-Hove singularity at the band-edge we first study the Bethe DOS [Eq. (9)]. To solve Eq. (11) for ω^* we insert Eqs. (8) and (6) and obtain

$$\frac{\partial A}{\partial U} \propto \left[\frac{dG_0(z)}{dz} \left(\frac{\partial \mu}{\partial U} - \frac{\partial \Sigma(\omega^*)}{\partial U} \right) \right]''_{z=\omega^*+\mu-\Sigma(\omega^*)} = 0. \tag{20}$$

Here the chemical potential μ has to be differentiated with respect to U because the spectrum in (11) corresponds to a given density. One can use Eq. (10) to rewrite this derivative as $\partial\mu/\partial U = \partial\Sigma(0)/\partial U$. From Eq. (10) and the fact that the first-order self-energy Σ_H is static, it follows that $\mu - \Sigma(\omega) = \mathcal{O}(U^2)$ for $U \to 0$. Thus $\partial\mu/\partial U - \partial\Sigma/\partial U$ vanishes identically. In particular one has $\mu - \Sigma(\omega) = -U^2\Sigma_2(\omega) + \mathcal{O}(U^4)$ for half-filling. However, instead of looking for a sign change in $\partial A/\partial U$ as in Eq. (11) one can more conveniently investigate the sign changes in $\partial A/\partial(U^2)$. Eq. (20) for the crossing frequency at $U = 0$,

$$\omega_0 \equiv \lim_{U \to 0} \omega^*(U) \tag{21}$$

then becomes

$$\frac{\partial A}{\partial (U^2)} \propto \Sigma_2''(\omega^*) \left(\frac{dG_0}{dz} \right)'_{z=\omega^*} + \Sigma_2'(\omega^*) \left(\frac{dG_0}{dz} \right)''_{z=\omega^*} = 0. \tag{22}$$

For the Bethe DOS the non-interacting Green function (7) and its derivative dG_0/dz are given in analytical form as

$$G_0(z) = 2(z - \sqrt{z-1}\sqrt{z+1}), \qquad \frac{dG_0}{dz} = 2 - \frac{2z}{\sqrt{z-1}\sqrt{z+1}}, \tag{23}$$

where the complex square root denotes the principal branch. When solving Eq. (20) for small U, special care has to be taken to handle the singularity of dG_0/dz at the band-edges correctly. The leading contribution is given by

$$\left. \frac{dG_0}{dz} \right|_{z=\omega+i0} \sim \begin{cases} i\frac{\sqrt{2}}{\sqrt{1-\omega}} & \text{for} \quad \omega \uparrow 1, \\ \frac{-\sqrt{2}}{\sqrt{\omega-1}} & \text{for} \quad \omega \downarrow 1. \end{cases} \tag{24}$$

The perturbative self-energy $\Sigma_2(\omega)$ is continuous and at least differentiable once as seen from Eqs. (18) and (19). To obtain $\partial A/\partial(U^2)$ close to $\omega=1$ we can thus replace Σ_2 by its value at the band-edge, $\Sigma_2''(1)\equiv v_2\approx -0.2926$ and $\Sigma_2'(1)\equiv u_2\approx -0.0692$. The result is

$$\frac{\partial A(\omega)}{\partial U^2}\sim\begin{cases}\frac{\sqrt{2}}{\sqrt{1-\omega}}\,u_2 \text{ for } & \omega\uparrow 1,\\ \frac{-\sqrt{2}}{\sqrt{\omega-1}}\,v_2 \text{ for } & \omega\downarrow 1\end{cases} \tag{25}$$

for $U\to 0$. Because $v_2/u_2>0$ this implies a sign change of the derivative $\partial A/\partial(U^2)$ at $\omega=1$, and thus the crossing point tends towards the band-edge in the limit of small U.

Because the self-energy has an expansion only in even powers of U one might expect that the same is true also for the crossing point $\omega^*(U)$ as a function of U. In particular, this would imply that for small U the crossing frequency varies only weakly in the sense that the linear term $\omega^*\sim U$ is absent. On the other hand, the square root in $G_0(z)$ at $z=1$ may cause $\omega^*(U)$ to become nonanalytic at $U=0$. However, as we will now show that these nonanalytic contributions occur only in higher order terms, and that the solution of (20) for small U is of the type

$$\omega^*=1+aU^2+\mathcal{O}(|U|^3). \tag{26}$$

To single out the nonanalyticity of dG_0/dz in Eq. (20) we introduce the notation $\omega^*=1+\delta\omega$ and $z=\omega^*-\Sigma(\omega^*)\equiv 1+\delta z$, i.e., $\delta z=\delta\omega-\Sigma(\omega^*)$. Eq. (20) then reads

$$1=\left(\delta z^{-\frac{1}{2}}\right)''C_1+\left(\delta z^{-\frac{1}{2}}\right)'C_2, \tag{27}$$

where we introduced

$$C_1=\left(\frac{1+\delta z}{\sqrt{2+\delta z}}\frac{\partial(\Sigma-\Sigma_{\mathrm{H}})}{\partial U}\right)'\Big/\left(\frac{\partial(\Sigma-\Sigma_{\mathrm{H}})}{\partial U}\right)'', \tag{28}$$

$$C_2=\left(\frac{1+\delta z}{\sqrt{2+\delta z}}\frac{\partial(\Sigma-\Sigma_{\mathrm{H}})}{\partial U}\right)''\Big/\left(\frac{\partial(\Sigma-\Sigma_{\mathrm{H}})}{\partial U}\right)''. \tag{29}$$

Let us now write $\delta z\equiv re^{i\phi}$ whence we obtain

$$\sqrt{r}=C_2\cos\frac{\phi}{2}-C_1\sin\frac{\phi}{2}. \tag{30}$$

With the ansatz (26) one has $\sqrt{r}=\mathcal{O}(|U|)$ and $\tan\phi=\delta z''/\delta z'\sim -v_2/(a-u_2)+\mathcal{O}(|U|)$ as $U\to 0$, whereas $C_1=v_2/u_2+\mathcal{O}(U^2)$ and $C_2=1+\mathcal{O}(U^2)$. Thus (26) solves Eq. (20) provided that

$$v_2\cos\frac{\phi}{2}-u_2\sin\frac{\phi}{2}\to 0 \tag{31}$$

for $U \to 0$. The solution of this, $\tan(\phi/2) \to v_2/u_2$, together with the behavior of $\tan\phi$ noted above, yields after some manipulation

$$a = \frac{u_2}{2}\left(1 + \frac{v_2^2}{u_2^2}\right) = 0.653. \tag{32}$$

The results of this section are easily generalized for any non-interacting DOS with a van-Hove singularity $\rho(\omega) \sim \sqrt{|\omega - W|}$ at the band-edge $\omega = \pm W$, as, e.g., for the DOS for a simple cubic lattice. This is because the dependence of $G_0(z) = \int d\epsilon\, \rho(\epsilon)/(z-\epsilon)$ and $dG_0/dz = -\int d\epsilon\, \rho(\epsilon)/(z-\epsilon)^2$ on $\rho(\epsilon)$ is linear. The singular part of $dG_0(z)/dz$ can be split off and the remaining continuous part does not enter the first-order result for ω^*. We thus conclude that a van-Hove singularity at a band-edge implies that in its vicinity a crossing point in the spectrum exists for small U, provided that $\Sigma_2'(1)$ and $\Sigma_2''(1)$ have the same sign.

3.3. Model Density of States

The situation is different if there is no van-Hove singularity at the band-edge of the non-interacting DOS, e.g., if the DOS vanishes linearly. In this case its derivative at the band-edge does not diverge. Then the weak-coupling crossing point ω_0 need not be located at the band-edge. We now demonstrate this by investigating the family of model functions

$$\rho_\alpha(\epsilon) = \frac{\alpha+1}{2\alpha W}(1 - |\epsilon/W|^\alpha)\Theta(W - |\epsilon|), \quad W = 1, \alpha = 1, 2, 3, \ldots \tag{33}$$

as non-interacting DOS. Here $\Theta(x)$ is the step function and again the half band-width $W = 1$ has been chosen as energy unit.

The functions $\rho_\alpha(\epsilon)$ are all linear at the band-edges but become increasingly steep as α increases (Fig. 4(a)). In the limit $\alpha \to \infty$ $\rho_\alpha(\omega)$ approaches the box-shaped DOS $\rho_\infty(\omega) = \Theta(1 - |\omega|)/2$, for which a similar calculation as in the last section shows that $\omega_0 = \pm 1$. We therefore write $\omega_0^{(\alpha)} = 1 - \Delta_\alpha/\alpha$ for the crossing frequency in the limit $U \to 0$ for the DOS $\rho_\alpha(\epsilon)$. As shown in the following, $\Delta_\alpha \to \Delta_0$ for $\alpha \to \infty$, i.e., there are corrections of the crossing frequency with respect to the band-edge, but these corrections become small as the DOS develops a discontinuity there.

We first write Eq. (22) as

$$\left.\frac{(dG_0/dz)'}{(dG_0/dz)''}\right|_{z=1-\Delta_\alpha/\alpha+i0} = -\left.\frac{(\Sigma_2^{(\alpha)})'}{(\Sigma_2^{(\alpha)})''}\right|_{z=1-\Delta_\alpha/\alpha+i0}. \tag{34}$$

The second-order contribution to the self-energy is shown in Fig. 4(b). Similar to the last section, the non-analytic behavior of dG_0/dz at $z = 1$

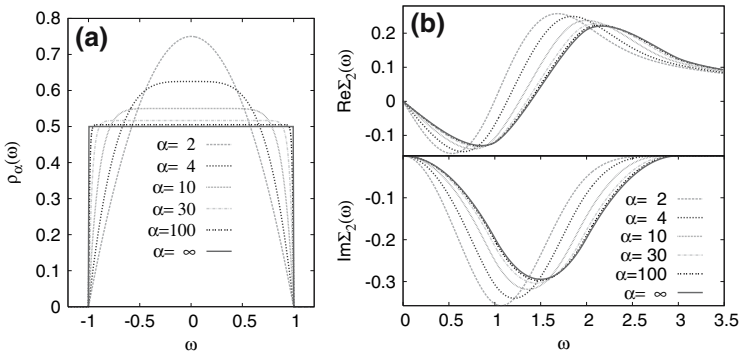

Fig. 4. (Color online) (a) The model DOS given by Eq. (33). (b) The corresponding second order self-energies $\Sigma_2(\omega)$.

determines the behavior of the solutions of this equation. For $\Delta_\alpha \ll \alpha$ and $\alpha \to \infty$ the leading contribution to the derivative [see Eq. (7)]

$$\frac{dG_0}{dz} = \frac{\alpha+1}{2\alpha} \int_{-1}^{1} dx \, \frac{1-x^\alpha}{(1-\frac{\Delta_\alpha}{\alpha}+i0-x)^2} \tag{35}$$

is given by

$$\frac{dG_0}{dz} \sim -\frac{\alpha}{2}\left(\frac{1}{\Delta_\alpha} + \mathrm{Re}\int_0^\infty dx \, \frac{e^{-x}}{(x-\Delta_\alpha+i0)^2} + i\pi e^{-\Delta_\alpha}\right). \tag{36}$$

On the other hand the right-hand side of (34) is finite for $\alpha \to \infty$. We can thus analyze the behavior of the solutions for large α by letting $\Delta_\alpha \to 0$ and $\alpha \to \infty$ in $\Sigma_2^{(\alpha)}|_{1-\Delta_\alpha/\alpha}$. To lowest order we then have

$$\omega_0^{(\alpha)} = 1 - \Delta_0/\alpha, \tag{37}$$

where Δ_0 is the a solution of

$$e^{\Delta_0}\left(\frac{1}{\Delta_0} + \mathrm{Re}\int_0^\infty dx \, \frac{e^{-x}}{(x-\Delta_0+i0)^2}\right) = \pi \left.\frac{(\Sigma^{(\infty)})''}{(\Sigma^{(\infty)})'}\right|_{\omega=1}. \tag{38}$$

Since $\Sigma_2^{(\infty)}(\omega)$ can be calculated directly from Eq. (18) and (19) we can solve (38) numerically. The result, $\Delta_0 = 0.0750$, is compared in Fig. 5 to a direct numerical solution of of Eqs. (18), (19), and (11), which is possible for not too large α. Figure 5 clearly demonstrates that in the limit $U \to 0$ the crossing points are not located at the band-edges if there is no van-Hove singularity.

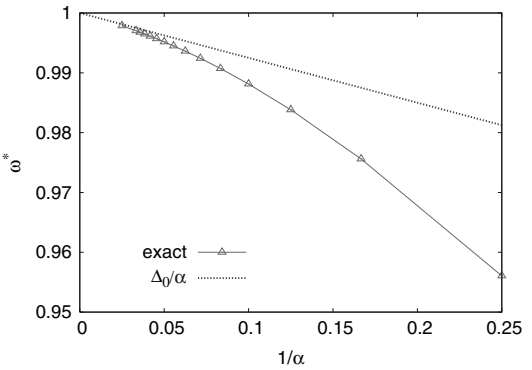

Fig. 5. (Color online) Location of crossing points in the spectral function in the limit $U \to 0$ for the non-interacting DOS $\rho_\alpha(\epsilon)$ [Eq. (33)]. The triangles mark the numerical solution of Eq. (11), the dotted lines shows the lowest order approximation [Eq. (37)].

4. CONCLUSION

In this paper, we presented an analytical investigation of isosbestic points in the local spectral function $A(\omega, U)$ of correlated electrons described by the Hubbard model. The existence of such crossing points in the curves of $A(\omega, U)$ versus ω for different values of the interaction U is due to sum rules for $A(\omega, U)$. For small U the frequency corresponding to the isosbestic point may be derived within weak-coupling theory. In particular we showed that if the non-interacting DOS has a van-Hove singularity at the band-edge, there is in general a crossing point at $\omega^* = W + \mathcal{O}(U^2/W)$ for $U \to 0$. By contrast, if the DOS vanishes linearly at the band-edge the crossing frequency is located at $\omega^*(U=0) \neq W$.

We established that, in general, the crossing frequency ω^*, and thus the value of the local spectral function at the crossing point, $A(\omega^*)$, sensitively depends on the form of the non-interacting DOS $\rho(\epsilon)$ at the band-edges. This is quite different from the near-universality of the crossing point values of the specific heat at high temperatures.[13] We therefore conclude that the study of isosbectic points in *dynamical quantities* can provide valuable information about microscopic energy scales of strongly correlated electron systems, e.g., the bandwidth of the non-interacting system.

ACKNOWLEDGMENTS

We thank Ralf Bulla for providing us with his NRG data and Krzysztof Byczuk for discussions. This work was supported in part by the DFG Sonderforschungsbereich 484.

REFERENCES

1. G. Scheibe, *Angew. Chemie* **50**, 212 (1937).
2. M. D. Cohen and E. Fischer, *J. Chem. Soc.*, **2**, 3044 (1962).
3. Isosbestic: from Greek *isos* "equal" + *sbestos*, verbal adjective from *sbennynai* "to quench, extinguish."
4. D. Vollhardt, *Phys. Rev. Lett.* **78**, 1307 (1997).
5. D. Greywall, *Phys. Rev. B* **27**, 2747 (1983).
6. G. E. Brodale, R. A. Fisher, N. E. Phillips, and J. Flouquet, *Phys. Rev. Lett.* **56**, 390 (1986).
7. H. G. Schlager, A. Schröder, M. Welsch, and H. von Löhneysen, *J. Low Temp. Phys.* **90**, 181 (1993).
8. H. Shiba and P. A. Pincus, *Phys. Rev. B* **5**, 1966 (1972); H. Shiba, *Progr. in Theor. Phys.* **48**, 2171 (1972).
9. G. Jüttner, A. Klümper, and J. Suzuki, *Nucl. Phys. B* **522**, 471 (1998).
10. D. Duffy and A. Moreo, *Phys. Rev. B* **55**, 12918 (1997); **56**, E7022 (1997).
11. A. Georges and W. Krauth, *Phys. Rev. B* **48**, 7167 (1993).
12. F. Gebhard and E. Ruckenstein, *Phys. Rev. Lett.* **68**, 244 (1991); F. Gebhard, A. Girndt, and A. Ruckenstein, *Phys. Rev. B* **49**, 10926 (1994).
13. N. Chandra, M. Kollar, and D. Vollhardt, *Phys. Rev. B* **59**, 10541 (1999).
14. S. Uchida, T. Ido, H. Takagi, T. Arima, Y. Tokura, and S. Tajima, *Phys. Rev. B* **43**, 7942 (1991).
15. J. K. Freericks, T. P. Devereaux, and R. Bulla, *Phys. Rev. B* **64**, 233114 (2001); J. K. Freericks, T. P. Devereaux, R. Bulla, and Th. Pruschke, *Phys. Rev. B* **67**, 155102 (2003).
16. J. K. Freericks and V. Zlatić, *Rev. Mod. Phys.* **75**, 1333 (2003).
17. K. Slevin, P. Markoš, and T. Ohtsuki, *Phys. Rev. B* **67**, 155106 (2003).
18. M.-F. Pouët, E. Baures, S. Vaillant, and O. Thomas, *Appl. Spectrosc.* **58**, 486 (2004).
19. R. W. Johnson, S. Susman, and D. L. Price, *J. Non-Crystalline Solids* **75**, 57 (1985).
20. W. Metzner and D. Vollhardt, *Phys. Rev. Lett.* **62**, 324 (1989).
21. A. Georges and G. Kotliar, *Phys. Rev. B* **45**, 6479 (1992).
22. D. Vollhardt, in: *Correlated Electron Systems*, V. J. Emery (ed.), World Scientific, Singapore (1993), p. 57.
23. Th. Pruschke, M. Jarrell, and J. K. Freericks, *Adv. Phys.* **44**, 187 (1995).
24. A. Georges, G. Kotliar, W. Krauth, and M. J. Rozenberg, *Rev. Mod. Phys.* **68**, 13 (1996).
25. G. Kotliar and D. Vollhardt, *Phys. Today* **57**, 53 (2004).
26. R. Bulla, A. C. Hewson, and Th. Pruschke, *J. Phys.: Condens. Matter* **10**, 8365 (1998).
27. R. Bulla, T. A. Costi, and D. Vollhardt, *Phys. Rev. B* **64**, 045103 (2001).
28. N. Blümer, Ph. D. thesis, Universität Augsburg (2002); Shaker (Aachen, 2003).
29. E. Müller-Hartmann, *Z. Phys. B* **76**, 211 (1989).
30. H. Schweitzer and G. Czycholl, *Z. Phys. B* **83**, 93 (1991).
31. F. Gebhard, E. Jeckelmann, S. Mahlert, S. Nishimoto, and R. M. Noack, *Eur. Phys. J. B* **36**, 491 (2003).